

Optimization analysis of Nd: YAG laser self-fluxing welding of Titanium alloy/stainless steel dissimilar metal by RSM

Y. F. ZHANG^{a,b,*}, H. ZHANG^a, H. T. ZHANG^a, Z. Q. ZHU^a, J. L. PAN^a

^aKey Laboratory for Robot & Welding Automation of Jiangxi Province, School of Mechanical & Electrical Engineering, Nanchang University, Nanchang 330031, China

^bSchool of Mechanics & Materials Engineering, Jiujiang University, Jiujiang 332005, China

The tensile load, weld depth-to-width ratio and IMCs layer thickness response value of 304 stainless steel / Ti6Al4V titanium alloy dissimilar metal joint under Nd: YAG pulsed laser self-fluxing welding condition were obtained by using the RSM of Box - Behnken design experiment. A multivariate nonlinear regression mathematical model was established by using the stepwise regression method to screen out the significant factors affecting the responses. The variance analysis and regression analysis show that the regression model probability $\Delta Prob > \Delta F$ is less than 0.001, which indicates that the regression equation can simulate the real surface well. The results show that there is a linear proportional relationship between the tensile load and the weld depth-to-width ratio/the IMCs layer thickness. The influence of the process parameters on the tensile load has a very complex interaction. Different from the similar metal welding, to obtain the maximum limit strength requires longer pulse width, smaller pulse repetition rate and welding current. The maximum tensile load is 705.008N under the optimum parameters of welding current 122A, pulse width 15ms and pulse repetition rate 2HZ. Under the optimal parameters, there is no macroscopic crack in the welded joint, and the evenly distributed IMCs along the welding interface exhibits 3 layers of color distinctly different microstructure. The welds interface generates α -Ti, TiFe, TiFe₂ and a small amount of Ti₅Cr₇Fe₁₇ IMCs. The order of precipitation is Ti₅Cr₇Fe₁₇, C14_Laves (TiFe₂) and BCC_B2 (TiFe). The brittle cleavage fracture of the welded joints occurs under normal stress. The fracture occurs in the fusion zone, breaking along the TiFe and TiFe₂ IMCs layers, and the fracture forms many secondary cracks.

(Received March 14, 2018; accepted April 8, 2019)

Keywords: RSM, ND, YAG pulsed laser self-fluxing welding, Titanium alloy, Stainless steel

1. Introduction

Titanium alloy has the characteristics of high specific strength, high temperature resistance and corrosion resistance, etc. It is mainly used in the manufacture of aircraft engine parts, the rockets, missiles and high-speed aircraft structural parts. It is also widely used in general industrial field, such as Electrolytic Electrode, power plant condenser, oil refining, desalination heater, environmental pollution control devices, production of hydrogen storage materials and shape memory alloy, etc. At present, Ti6Al4V titanium alloy accounts for 50% of total titanium production, accounting for 95% of all titanium alloy processing parts. Because of its high strength and better plasticity, Ti6Al4V titanium alloy is the most important veteran alloy used in aerospace industry [1]. But the relatively high price of titanium alloy restricts its wider application. Steel has the characteristics of good weldability, mechanical properties and low cost, etc. It is the most widely used metal material. With some steel instead of titanium alloy can effectively take into account the

advantages of both materials to give full play to the advantages of two kinds of metal materials. Such as: titanium alloy with greater adaptability in harsh work or in the biological tissue environment. At this point the titanium alloy structure matrix can use stainless steel, contact with the harsh conditions of the interface with titanium alloy. This will not only ensure the structural needs of the work, but also reduce the usage of titanium alloy, improving the economy. Therefore, the titanium alloy / steel dissimilar metal welded structure is favored. It is widely used in the aerospace, marine engineering and biomedical fields and other fields. One of the most typical application is in the chemical industry for the manufacture of high temperature, high pressure and strong corrosion and other special chemical equipment, such as concentration tower, reactor, heat exchanger and oxidation reaction condenser and so on. In the ship, titanium alloy / steel welded structure not only satisfies the strength requirements but also resists corrosion.

The thermal physical and chemical properties of titanium alloy and stainless steel are quite different. In particular, the solubility of Fe in Ti is very small at room

temperature, Ti and Fe easily form hard and brittle IMCs. As a result, titanium alloy / stainless steel welding is very difficult [2]. Moreover, titanium is easy to form complex IMCs and carbides with elements such as Cr, Ni and C in steel, leading to serious embrittlement of welded joints, and even crack generation. In addition, the chemical activity of titanium is high, and it increases sharply with the rise of temperature. Titanium absorbs hydrogen, oxygen and nitrogen rapidly, which makes the joints brittle at 250°C to 600°C high temperature. Therefore, strict cleaning is needed before welding and strict protection measures should be taken during the welding process. For titanium alloys / steel, the methods to achieve connection are mainly adhesive connection, mechanical connection and welding [3]. For adhesive connection, the joint strength is limited and is only applicable where the strength requirements is low. For mechanical connection, the joint strength is high, but the joint quality and air tightness cannot be guaranteed. Welding is an effective way to connect components at the same time to meet all aspects of performance requirements. But the materials thermal physical properties are obviously different and the metallurgical compatibility is poor. At present, a transition layer for fusion welding, the interface pre-intermediate layer for pressure welding or with expensive silver-based solder for brazing and other technology means are used for the dissimilar metal welding [4-6]. The filler metal is used to prevent the diffusion of alloying elements between Ti and steel to form IMCs. In Diffusion welding process, adding middle layer can also effectively reduce the formation of intermetallic compounds, which plays a role in improving the performance of welded joints. Commonly used intermediate layer materials are copper, copper-based alloys, vanadium, nickel and aluminum [7-9]. Ghosh, M., et al. [10, 11] were respectively subjected to diffusion welding and vacuum brazing experiments on titanium alloy / stainless steel. Although joint strengths of diffusion welding, and brazed welded are better, but the welding atmosphere is sensitive, which usually needs a vacuum environment.

But the conventional fusion welding method is difficult to achieve effective connection due to the large amount of heat input and low heat source control accuracy [12]. Brazing welding cycle is long, welding flexibility is poor, and joints performance is not high. Pressure welding is difficult to meet the needs of mass production due to being affected by the shape and size of the workpiece, the need for process assembly and low welding efficiency [13]. It is necessary to carry out research on new technology of titanium alloy / steel welding. The traditional fusion welding method to form the welded joint is through the heat conduction and convection way to heat transfer to the workpiece so that the local area is melted and solidified, while the laser welding to achieve the joint connection is the deposition of heat energy on the workpiece surface through the interaction of optical radiation (laser beam) with the

material. The laser welding energy input response conforms to the law of optics, which shows that the welding has the advantages of high time stability, good spatial distribution flexibility and easy adjustment of the beam, etc. With the development of science and technology, the laser is more efficient in terms of time stability, spatial distribution flexibility and energy consumption. Laser welding using laser beam as welding energy has the advantages of fast welding speed, process stability, high energy density and small welding deformation, etc. As the laser spot diameter is small and the local area energy density is high in the dissimilar metal welding process, which can significantly improve the welding speed and reduce the molten pool diameter. The rapid crystallization of the molten pool due to the large temperature gradient in the laser welding process reduces the degree of segregation and limits the growth of intermetallic compounds [14-17]. Laser welding has become an important technical means for high quality and efficient connection of titanium alloy / steel dissimilar metals. Hiraga, H., et al. [18] has been welded to titanium alloy / stainless steel tube by YAG laser, the results show that only the titanium tube is located inside the lap joint to ensure that the welded pipe joint is tight and does not leak. Chen, S., et al. [19] studied the effect of CO₂ laser beam offset on microstructure and fracture behavior of titanium alloy / stainless steel butt joint, the results show that the tensile strength of the joint is higher when the laser beam is biased towards the titanium alloy side. The intermetallic compounds are evenly divided into two layers along the interface, one layer is TiFe + α -Ti and the other layer is TiFe + TiFe₂+Ti₅Fe₁₇Cr₅. Zhang, Y., et al. [20, 21] studied the TC4 titanium alloy / SUS301L stainless steel pulsed laser butt welding with Nb as the middle layer. The laser beam is located near the titanium - Nb interface during the welding process. The results show that there is no Ti-Fe intermetallic compounds in the weld, and Nb effectively prevents the mutual diffusion and reaction between Ti and Fe. The fracture occurs at the interface reaction layer of Nb-stainless steel. Tomashchuk, I., et al. [22-24] uses V and Cu as the intermediate layer to realize the effective connection of AISI 316L stainless steel / Ti6Al4V titanium alloy butt joint by continuous laser welding and electron beam welding. The results show that the high cooling rate of laser welding has a certain inhibitory effect on the σ -crack sensitive phase formed by Fe and V. The pure copper intermediate layer reduces the formation of brittle Ti-Fe and Ti-Cr phases, Cu-Ti and Cu-Fe-Ti phases have little effect on the weld strength, and the CuTi₂+TiFe+ α -Ti brittle layer formed in the weld reduces the joint strength. Titanium alloy/steel dissimilar metal laser welding-brazing has the following problems: Lack of matching the solder simultaneously with the titanium alloy and steel, And the wettability between the liquid solder and the base material is poor, welding need to use flux to improve spreadability, which bring certain impacts to the weld forming and welding process stability,

it is difficult to achieve all-position welding. Brazed seam and base metal did not achieve metallurgical bonding, joint performance is low. With the laser output power rising, laser penetration welding will increase in the laser welding field. However, there are many adjustable process parameters of laser welding, and there are interaction between each factor. It is very important to find out the influence of each process parameter on the performance of joint.

The response surface method (RSM) is based on the multivariate nonlinear regression mathematical model to establish the relationship between the response and the input factors. The goal is to optimize the response or to understand the deep mechanism of statistical methods, which was introduced by Box and Wilson in the 1850s [25]. The second-order design includes central composite design, Box-Behnken design and uniform shell design. Box-Behnken design is less than the number of central composite design trials under the same factors, which does not combine all the experimental factors at the same time as a high level of experimental combination, which is adapted to experiments with safety requirements or special needs. Which has an approximate rotation, no sequential[26]. For this reason, titanium alloy / steel

dissimilar metal laser lap welding process scheme was formulated via Box - Behnken design, using the RSM to analyze the test data, the second-order mathematical equations relation between the laser welding process parameter (pulse current, pulse duration and Pulse repetition rate) and the predicted response value (joint tensile load, weld depth-to-width ratio and IMCs layer thickness) is established. The welding process parameters were optimized, the tensile load, the depth-to-width ratio and the IMCs layer thickness of the dissimilar metal lap welded joint were predicted by the multivariate nonlinear regression mathematical model, and to establish a functional relationship between them. The working parameters of the dissimilar metal laser welding were provided, and the mechanism of joining and IMCs formation were studied.

2. Experimental method

304 stainless steel and Ti6Al4V titanium alloy sheets with size of 100mm × 50mm × 0.5mm were selected as the raw materials. Their chemical compositions were listed in Table 1.

Table 1. Chemical composition of experimental material

Alloy	Chemical composition (wt.%)								
304SS	C	Si	Mn	P	S	Ni	Cr	Fe	
	0.071	0.57	1.53	0.028	0.027	8.02	17.51	balance	
Ti6Al4V	Al	V	Fe	Si	C	N	H	O	Ti
	5.500-6.800	3.500-4.500	0.300	0.1500	0.100	0.050	0.015	0.150	balance

The Nd: YAG laser welding equipment is produced by BeiJing Zhengtian Hengye CNC Technology Co., and the machine model is ZT-H-700W. The model device parameters are that maximum output power is 700 W, wavelength of Nd: YAG laser beam is only 1.064μm and laser spot size *d* is 1.0±0.3 mm. The narrow pulsed laser beam can deposit the energy beam in a very small area. The melting point of the Ti6Al4V titanium alloy and the 304 stainless steel is about 1600 °C and 1400 °C respectively. Because the welding base metal has different melting point, the density of the titanium alloy is relatively low, and the laser absorptivity is higher, therefore, the lap joint form of titanium alloy in upper of steel was taken. This method can effectively reduce the mixing of the two materials at the interface, control the mutual diffusion of Ti and Fe elements, inhibit the formation of IMCs and improve the weld strength. In order to evaluate the quantitative relationship between the laser welding process parameters and the predicted response values and to optimize the welding process parameters. Titanium alloy / steel dissimilar metal laser

lap welding process was formulated via Box - Behnken design.

The RSM characterizes the relationship between one or more responses and input factors. When all the independent variables are controllable, measurable and continuous in the experiment, then the error is ignored in the case, the RSM can be expressed as:

$$y=f(x_1,x_2,\dots,x_k) \tag{1}$$

where *k* is the number of independent variables.

The key to optimizing the response *y* is to find a suitable approximation to satisfy the function of the independent variable and the response surface, usually using the second-order model in the RSM.

$$y = \beta_0 + \sum_{i=1}^k \beta_i x_i + \sum_{i<j}^k \beta_{ij} x_i x_j + \sum_{i=1}^k \beta_{ii} x_i^2 + \varepsilon \tag{2}$$

where *y* is the response, *x* is the independent factor, β_0 is

the constant term of the quadratic regression equation, β_i is the linear effect of x_i , β_{ij} is the linear \times linear interaction effect between x_i and x_j , β_{ii} is the quadratic effect of x_i .

The factor level codings used in the laser welding test were shown in Table 2. Among them, the table "0" represents the center point, "-" represents the next level, and "+" represents the upper level.

Table 2. Factor level codings and true value table of laser welding process parameters

level coding	Factor		
	Pulse current I (A)	pulse duration D (ms)	Pulse repetition rate f (HZ)
-	120	11	2
0	125	13	5
+	130	15	8

*Note: welding speed $v = 50\text{mm} / \text{min}$, defocus amount -1mm , argon flow $15\text{ L} / \text{min}$.

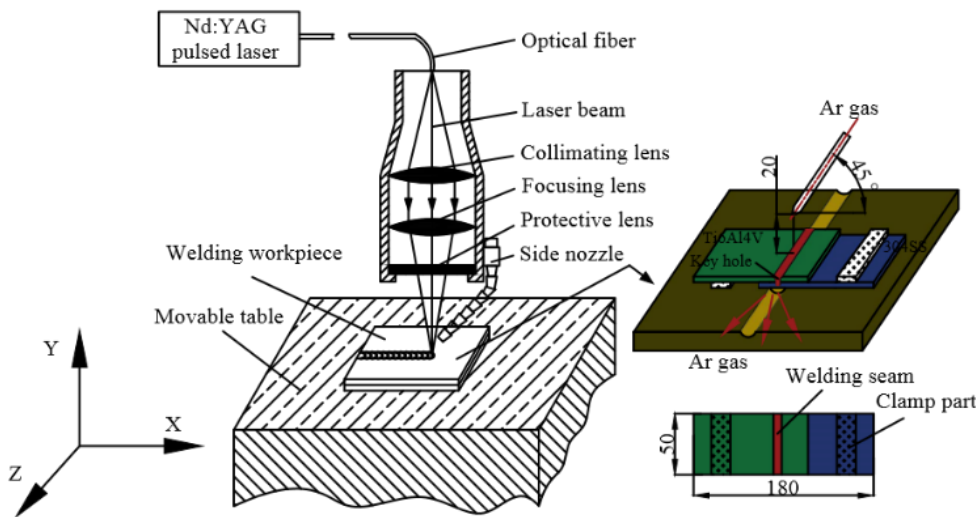


Fig. 1. Schematic diagram of laser welding equipment and protective gas nozzle positions

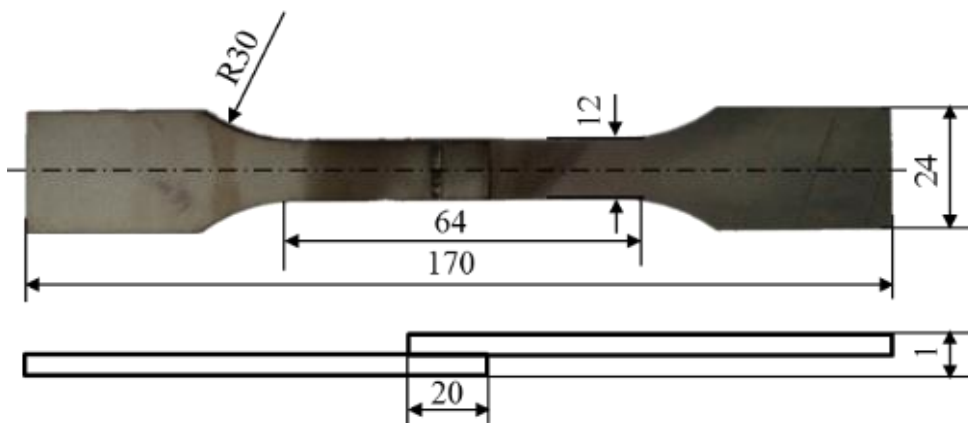


Fig. 2. The size of tensile specimen

Before welding, the workpiece surface oxide layer was polished with 320 # sandpaper, and lap joints near 15mm oil was removed with acetone. The workpiece was pre-tightened by tooling fixture during the welding process, which can effectively control the wave deformation of the sheet workpiece to ensure the value of

the welding defocus amount. The schematic diagram of laser welding equipment and protective gas nozzle positions are shown in Fig. 1. After welding, the weld depth-to-width ratio was calculated by measuring the weld penetration depth and the weld width. The quality of weld surface was evaluated by low magnification

metallographic microscope. The cross section of the joint was corroded by the etchant with $\text{FeCl}_3:\text{HCl}:\text{C}_3\text{H}_8\text{O}_3=1 \text{ g}:10 \text{ mL}:1 \text{ mL}$ and $\text{HF}:\text{HNO}_3:\text{H}_2\text{O}=1 \text{ mL}:3 \text{ mL}:7 \text{ mL}$. The weld IMCs layer was observed by SEM and its thickness was measured. The elemental content of the weld and the tensile fracture was analyzed by EDS. The interfacial phase composition was analyzed by XRD. Tensile specimens were prepared using a wire cutting machine in accordance with tensile standard for High -

Energy Beam Welded joints of Metallic Materials. The loading rate was 0.3 mm / min , and the standard tensile specimen was shown in Fig. 2. The fracture morphology was observed by SEM.

In order to avoid systematic errors, random secondary regression Box-Behnken design tests were performed. Laser welding test process parameters and results are shown in Table 3.

Table 3. Laser welding test parameters and response data

Experiment no.	mode	Pulse current $I(\text{A})$	pulse duration $D(\text{ms})$	Pulse repetition rate $f(\text{HZ})$	Tensile load $Y_1 \text{ (N)}$	depth-to-width ratio Y_2	IMCs $Y_3(\mu\text{m})$
1	--0	120.00	11.00	5.00	321.432	0.520	147.99
2	--0	120.00	15.00	5.00	465.084	0.370	127.96
3	0++	125.00	15.00	8.00	508.116	0.346	66.92
4	000	125.00	13.00	5.00	226.776	0.480	195.24
5	0-+	125.00	11.00	8.00	186.960	0.357	182.20
6	000	125.00	13.00	5.00	220.102	0.480	209.22
7	0+-	125.00	15.00	2.00	576.444	0.286	49.84
8	0--	125.00	11.00	2.00	240.828	0.504	254.28
9	-0-	120.00	13.00	2.00	689.304	0.449	68.66
10	++0	130.00	15.00	5.00	374.676	0.476	131.01
11	000	125.00	13.00	5.00	224.032	0.482	216.05
12	+0-	130.00	13.00	2.00	94.284	0.537	579.27
13	+0+	130.00	13.00	8.00	250.320	0.498	185.15
14	-0+	120.00	13.00	8.00	236.796	0.339	157.82
15	+0-	130.00	11.00	5.00	73.380	0.584	792.13

3. Results and analysis

3.1. Multiple quadratic mathematical model

The second-order model is the best fit model compared to the linear, 2FI and cube models in the case of highly significant P-value and without lack of fit. The least squares method was used to calculate the coefficients of the quadratic polynomial equation, and the mathematical model was established. The validity of the mathematical model was tested, and the fitting of the mathematical model at the test point was mainly checked.

The stepwise regression method was used to establish the multiple regression equation with joint tensile load, weld depth-to-width ratio and IMCs layer thickness as the response values, in which pulse current, pulse duration and pulse repetition rate as the factor. In the stepwise regression, stop the rule by Prob threshold 0.20 of entering the equation and the rejection probability,

the direction was mixed, and the rule was combined to carry out multiple nonlinear regression. The main effect I, D, f and the interaction items $I \times D, I \times f, D \times f, I \times I, D \times D$ and $f \times f$ were selected to construct the model effectively. This effect was removed from the model when an effect probability $\Delta\text{Prob} > \Delta F$ (significance) was greater than 0.20 during the effect screening process using the stepwise regression method. The effect estimates and $\Delta\text{Prob} > \Delta F$ values were shown in Table 4.

Multivariate nonlinear regression equation:

$$\begin{aligned}
 Y_1 = & 231.20 - 114.99 \times \frac{I-125}{5} + 137.72 \times \frac{D-13}{2} - 52.33 \times \frac{f-5}{3} + \\
 & 39.41 \times \frac{(I-125)}{5} \times \frac{(D-13)}{2} + 152.14 \times \frac{(I-125)}{5} \times \frac{(f-5)}{3} + \\
 & 71.76 \times \left(\frac{D-13}{2}\right)^2 + 80.80 \times \left(\frac{f-5}{3}\right)^2
 \end{aligned}
 \tag{3}$$

$$\begin{aligned}
 Y_2 = & 0.48 + 0.052 \times \frac{I-125}{5} - 0.061 \times \frac{D-13}{2} - 0.030 \times \frac{f-5}{3} + \\
 & 0.018 \times \frac{(I-125)}{5} \times \frac{(f-5)}{3} + 0.052 \times \frac{(D-13)}{2} \times \frac{(f-5)}{3} + \\
 & 0.045 \times \left(\frac{I-125}{5}\right)^2 - 0.038 \times \left(\frac{D-13}{2}\right)^2 - 0.070 \times \left(\frac{f-5}{3}\right)^2 \quad (4)
 \end{aligned}$$

$$\begin{aligned}
 Y_3 = & 201.77 + 148.14 \times \frac{I-125}{5} - 125.11 \times \frac{D-13}{2} - 45.00 \times \frac{f-5}{3} + \\
 & -160.27 \times \frac{I-125}{5} \times \frac{D-13}{2} - 120.82 \times \frac{I-125}{5} \times \frac{f-5}{3} + \\
 & 101.81 \times \left(\frac{I-125}{5}\right)^2 - 59.65 \times \left(\frac{f-5}{3}\right)^2 \quad (5)
 \end{aligned}$$

Tables 4 and 5 show the probability $\Delta\text{Prob} > \Delta F$ were less than 0.001 and the R^2 of the three fitting regression equations were more than 0.90, which indicates that the regression equation can simulate the real surface well. Figs. 3-5 show the three response scatter diagrams, indicating that the regression equation without lack of fit.

Table 4. Effect estimates and $\Delta\text{Prob} > \Delta F$ values table

Factor	Tensile load Y_1 (N)			depth-to-width ratio Y_2			IMCs Y_3 (μm)		
	Coefficient Estimate	$\Delta\text{Prob} > \Delta F$	Yes/No	Coefficient Estimate	$\Delta\text{Prob} > \Delta F$	Yes/No	Coefficient Estimate	$\Delta\text{Prob} > \Delta F$	Yes/No
Intercept	231.20	0.0002	Yes	0.48	0.0001	Yes	201.77	0.0005	Yes
I	-114.99	0.0003	Yes	0.052	0.0002	Yes	148.14	0.0003	Yes
D	137.72	0.0001	Yes	-0.061	< 0.0001	Yes	-125.11	0.0008	Yes
f	-52.33	0.0209	Yes	-0.030	0.0031	Yes	-45.00	0.0845	Yes
$I \times D$	39.41	0.1581	Yes	0	0.2531	No	-160.27	0.0015	Yes
$I \times f$	152.14	0.0005	Yes	0.018	0.0894	Yes	-120.82	0.0066	Yes
$D \times f$	0	0.9056	No	0.052	0.0010	Yes	0	0.5624	No
$I \times I$	0	0.7005	No	0.045	0.0027	Yes	101.81	0.0174	Yes
$D \times D$	71.76	0.0276	Yes	-0.038	0.0061	Yes	0	0.8344	No
$f \times f$	80.80	0.0168	Yes	-0.070	0.0003	Yes	-59.65	0.1124	Yes

Table 5. Model variance analysis table

Model	df	Cor Total	Mean	Sum of Squares	Mean Square	F Value	R-Squared	Adj R-Squared	Pred R-Squared	Adeq Precision
Y_1 (N)	7	14	312.57	4.187E+005	59817.55	24.03	0.9601	0.9201	0.6643	17.034
Y_2	8	14	0.45	0.10	0.013	41.70	0.9823	0.9588	0.8206	22.872
Y_3 (μm)	7	14	224.25	5.333E+005	76191.46	18.98	0.9500	0.8999	0.6609	16.537

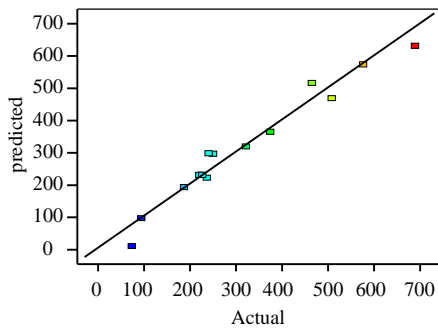


Fig. 3. Y_1 scatter diagram

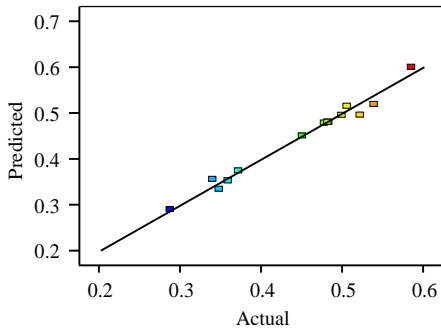


Fig. 4. Y_2 scatter diagram

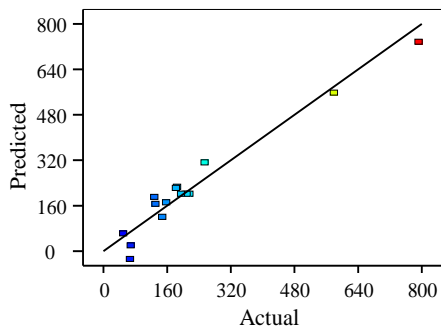


Fig. 5. Y_3 scatter diagram

3.2. Influence of process parameters on response value

The influence factors of the response values on the loading capacity of dissimilar metal welded joints include weld size, brittle layer thickness, splash, crack and porosity, etc. The main factors are weld size and brittle layer thickness. The weld tensile load is low when the actual bonding area of the joint is small in the low-aspect-ratio. And the weld tensile load is low when it increases in splashing, cracks, porosity and other welding defects with the increase of the brittle layer thickness in the high-aspect-ratio. From the multivariate nonlinear regression equation, Y_1 and Y_2 / Y_3 have similar linear proportional relationship. As shown in Fig. 6, it is shown that the influence of the welding process parameters on the tensile load is consistent with the influence of the

aspect-ratio/IMCs layer thickness. So this paper just covers the influence mechanism of the process parameters on the tensile load.

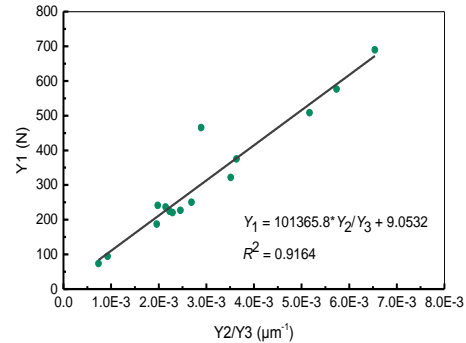


Fig. 6. Y_1 and Y_2/Y_3 linear fit graph

It can be seen from the regression model that the influence of the tensile load is divided into the main effect (linear term) and the interaction effect (cross term and quadratic term). The influence of each process parameter on the tensile load is not a simple superposition but a very complicated interaction. Based on the multivariate nonlinear regression equation, the 3-D response surface and contour plot of the influence of welding parameters on the response interaction were established. Taking the two-function variables of the model cross-term in the working range, the third function variables take the center value constant to establish the response surface plots, as shown in Figure7. Figure7a shows that the tensile load increases gradually with the increase of pulse width, and the larger current, the faster the rate of change. The tensile load decreases gradually with the increase of welding current, and the longer pulse duration, the slower the rate of change. The influence of pulse width on tensile load can be explained by weld geometry. When the pulse width was short, the bath did not have enough time to form, resulting in smaller weld size and actual bonding zone, which led to lower tensile load. The current size determined the mixing degree of the weld interface pool. The greater the current, the greater the mixing of the molten metal pool, causing the weld to form a large number of IMCs. Splash, cracks and porosity and other welding defects will also be a large number of formation. These synthetic factors have a strong impact on the loading capacity of the joint.

Fig. 7 b shows that the tensile load decreased gradually with the increase of welding current at $f < 7$ HZ, and the higher frequency, the slower the rate of change. The tensile load increased gradually with the increase of welding current at $f > 7$ HZ, but the trend is not obvious. The tensile load decreased gradually with the increase of pulse repetition rate at $I < 122$ A, and the larger current, the slower the rate of change. The tensile load decreased first and then increased with the increase of the pulse repetition rate at $I > 122$ A. The interaction between the

welding current and the pulse repetition rate on the tensile load can be explained by the overlapping factor.

The overlapping factor is a key factor in ensuring maximum load and air tightness for welded structural parts. Fig. 8 shows the overlapping factor of welding spots. The overlapping factor (O_f) between the welded spots is calculated as:

$$O_f = [1 - \frac{v}{f \times (d + vD)}] \times 100\% \quad (6)$$

where v is the welding speed (mm/s), f is the pulse repetition rate (HZ), d is laser spot size(mm), D is pulse duration.

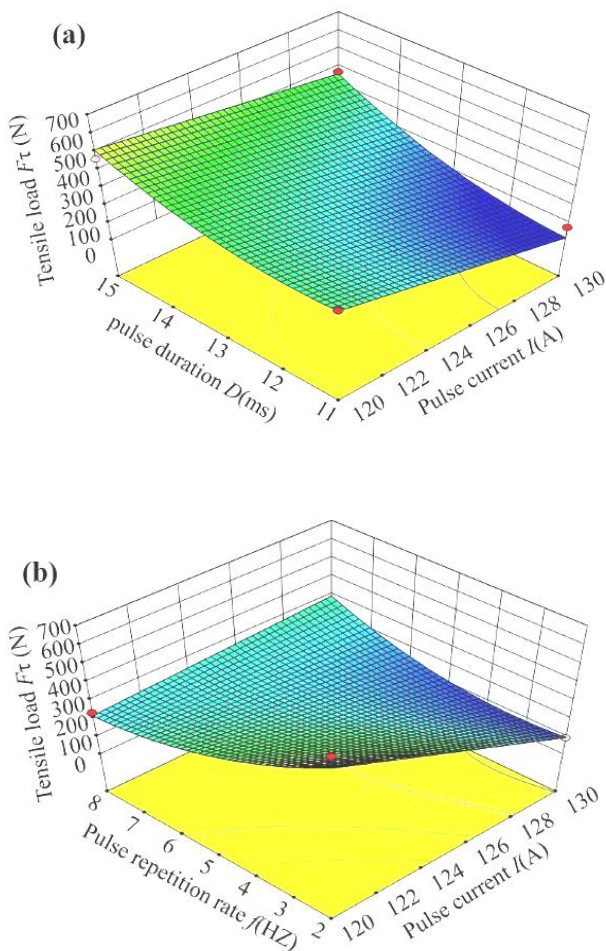


Fig. 7. 3D Response surface plots showing the interaction effects of (a) $I \times D$, (b) $I \times f$ on the tensile load

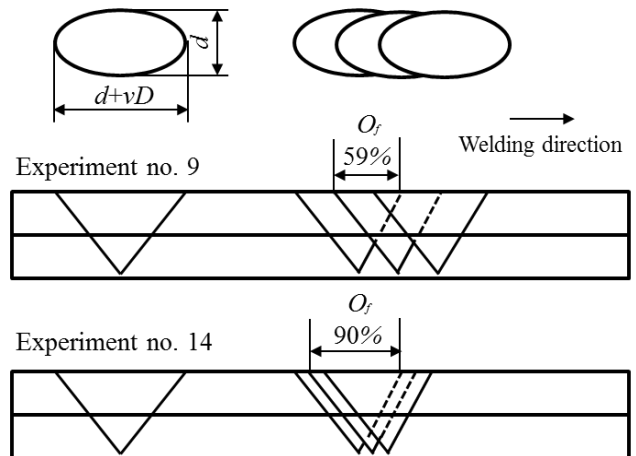


Fig. 8. Overlapping factor diagram along the welding path

From the overlapping factor function that the pulse repetition rate has the most significant effect on the overlapping factor at a certain welding speed and laser spot size, and the influence of pulse duration can be neglected. Therefore, the interaction between the overlapping factor and the welding current on the tensile load is the same as the interaction between the pulse repetition rate and the welding current on the tensile load. When O_f is 75%, the similar metal welding can get the maximum limit load [27], but this law does not apply to titanium alloy/steel dissimilar metal welding. Fig. 9 shows the effect of welding current on the surface forming of the joint at different overlapping factor. When O_f is 59 % (Fig. 9 a and b), the macro longitudinal through crack appears on the weld surface at the larger current, which results in a sharp decrease of the joint tensile load. When O_f is 90 % (Fig. 9 c and d), the surface crack of the weld is insensitive to the current change, and the tensile load has no significant change. When I is 120A (Fig. 9 a and c), the greater O_f , the smaller loading capacity of the joint. When I is 130A (Fig. 9b and d), the macro longitudinal through crack appears on the weld surface at the smaller O_f .

A single pulse weld geometry is a conical shape, and the surface has a large radiation surface. When O_f is 59 %, weld overlap only appears on the metal surface, no continuous penetration weld has been formed on the thickness of the entire joint, and the internal non-overlapping weld size is small. Under high current, the size of single pulse spot weld is relatively large, and the thermal stress of welding joint is extremely uneven, so that the surface longitudinal through crack occurs under the forced preload of fixture. The uneven distribution of the thermal stress is reduced in the small current, and the amount of the IMCs decreases, the welding defects are reduced, so that the joint has high strength. When O_f is 90 %, the continuous penetration weld has been formed on the thickness of the entire joint, the thermal stress distribution of the welded joint is

uniform and the surface crack sensitivity is decreased.

3.3. Numerical optimization

The statistical software optimization design is based on the established mathematical model which searches the design space to find any combination factor that optimizes one or more target responses. The optimal subset is determined as the test scheme in the candidate experimental points set by optimizing the algorithm. In this paper, the common optimization criteria sets the target for the maximum tensile load, and the welding

process parameters remain within the design space. Table 6 shows the criteria for numerical optimization. Table 7 shows the best five set of Pareto Optima parameter combinations for selected criteria. For optimum tensile loading, the optimum parametric range for I , D and f are 120.01-122.05 A, 13.92-14.99 ms and 2.01-2.28 HZ, respectively. It is concluded that the maximum limit strength of joint requires longer pulse width, smaller pulse repetition rate and welding current, so as to control the mixing degree of the weld interface pool and reduce the formation of IMCs and welding defects, while achieving a larger actual bonding area.

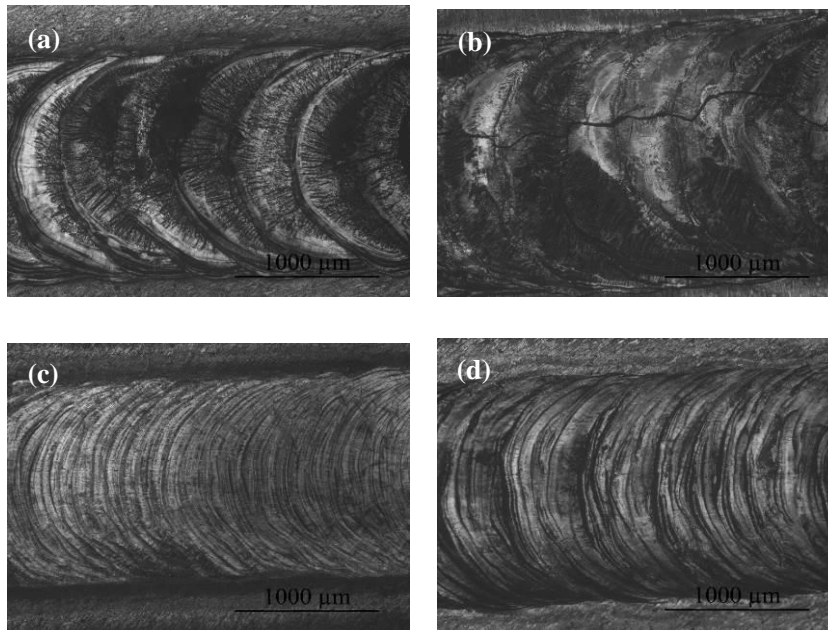


Fig. 9. Effect of welding current on surface forming at different overlapping factor; (a) $I=120$ A, $O_f=59\%$; (b) $I=130$ A, $O_f=59\%$; (c) $I=120$ A, $O_f=90\%$; (d) $I=130$ A, $O_f=90\%$

Table 6. The selected criteria for numerical optimization

Name	Goal	Limit		Importance
		Lower	Upper Limit	
I (A)	is in range	120	130	3
D (ms)	is in range	11	15	3
f (HZ)	is in range	2	8	3
$Y_1(N)$	maximize	73.38	689.304	4

In order to verify the rationality of the mathematical regression model, three experiments were carried out for each parameter. The response results obtained by the expected function analysis are experimentally verified.

Table 8 shows the relative error between the optimal response value and the experimental value is small, indicating the effectiveness of the optimization process.

Table 7. Optimal welding conditions based on the selected criteria

Sol. NO.	I (A)	D (ms)	f (HZ)	Y_1 (N)	Desirability
1	122.05	14.99	2.02	703.960	1.000 Selected
2	120.01	14.10	2.01	705.950	1.000
3	120.14	14.70	2.26	730.134	1.000
4	121.06	14.83	2.28	701.689	1.000
5	120.01	13.92	2.01	689.409	1.000

Table 8. Optimization validation test results

Optimum condition				Y_1 (N)	Y_2	Y_3 (μ m)
I (A)	D (ms)	f (HZ)				
122	15	2	Avg. Actual	705.008	0.316	40.03
			Predicted	703.960	0.288	34.643
			Error%	0.15	8.86	13.46

4. Microstructures and mechanical properties of the joint

The microstructures and mechanical properties of the joint in the optimum conditions were analyzed, and the mechanism of dissimilar metal laser welding connection and IMCs formation were studied.

4.1. Microstructure analysis

Fig. 10 shows the titanium alloy / steel laser lap weld cross-section back scattered electron imaging (BSE). It can be seen from the figure that the upper layer of titanium alloy is darker, the lower layer of stainless steel is brighter, and the interface color appears distribution feature alternate with brightness and darkness, which indicates that the laser has high temperature stirring effect on the molten pool, and mutual diffusion and migration of elements at the interface during the welding process. Titanium alloys and steel have melted in the laser radiation area (Fig. 10 a). The IMCs with uniform thickness distribution was formed on the interface between the titanium alloy and the stainless steel after welding. The total thickness of the IMCs was about 40 μ m. The entire welded joint has no macroscopic cracks, and there are 3 layers of color distinctly different microstructure on the lap interface.

The weld interface reaction layer structure can be divided into 3 layers (Fig. 10 b). The gray band region adjacent to the titanium alloy side can be called Layer I, the white band region of the interlayer can be called Layer II, and the acicular structure near the fused and

stainless steel interfaces can be called Layer III. The main component of the black distribution in the Layer I gray band region is Ti element. The relative content of Ti and Fe elements in the Layer II white band region is approximately the same, and the white component is mainly Fe element. The content of Fe element in the Layer III acicular structure is relatively high. From the Ti-Fe binary equilibrium phase diagram [28], the solid solubility of Fe in α -Ti is only 0.05% to 0.1% at room temperature and no more than 0.5% (mass fraction) at eutectoid temperature. By analyzing the composition, it is found that the two elements ratio of the weld interface exceeds the mutual dissolution range at room temperature, and it can be concluded that the Ti-Fe IMCs is formed in the weld interface area.

The EDS analysis of Ti, Al, V, Fe, Cr and Ni elements in different positions of the welds (Fig. 10 c), as shown in Table 9. It was found that the relative content of Ti and Fe in different positions was different, and the Fe content increased with the depth increasing in the fusion zone. From the Ti-Fe binary equilibrium phase diagram, the main component of zone 1 is the Ti element, which may form α -Ti phase. The main components of zones 2 and 4 are Ti and Fe, and the atomic ratio is close to 3: 1, which indicates that α -Ti and TiFe phases may be formed. The atomic ratios of Ti and Fe are close to 1: 1 in zones 3 and 5, which indicates that TiFe phase may be formed. The atomic ratio of Ti and Fe is close to 1: 2 in zone 6, which indicates that TiFe₂ phase may be formed. The atomic ratio of Ti, Cr and Fe is close to 5: 7: 17 in zone 7, which indicates that Ti₅Cr₇Fe₁₇ phase may be formed.

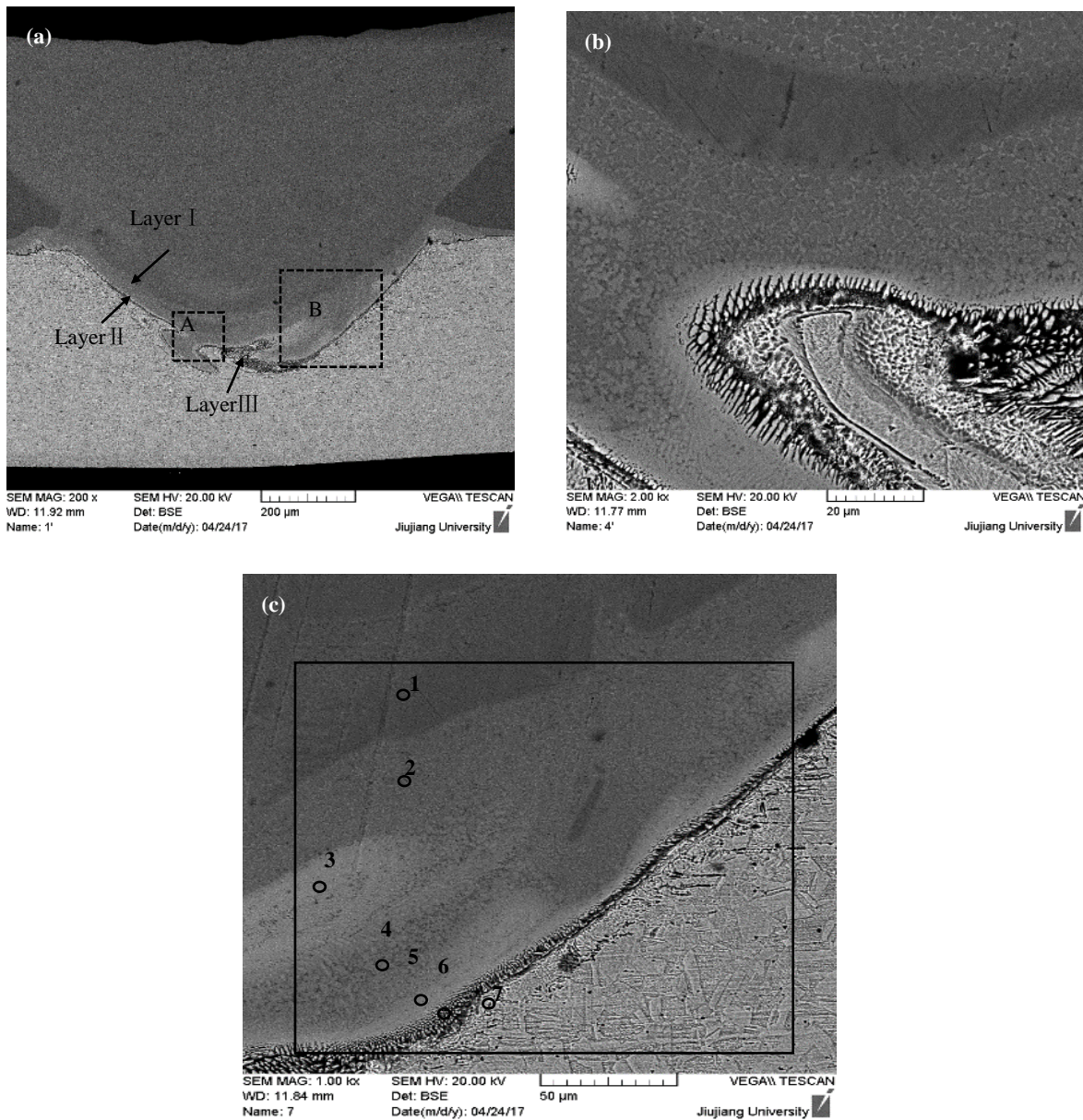


Fig. 10. BSE image of the joint. (a) macro cross-section (b) magnification in the A area and (c) magnification in the B area

The photos of weld area (Fig. 10c) scanned by EDS is shown in Fig. 11. It can be seen that the Fe element is diffused and migrated strongly to the titanium alloy side, and the diffusion distance is long. While the diffusion distance of the Ti element to the stainless steel side is short. The reason is that the Fe atom radius (0.127nm) is less than the Ti atom radius (0.147nm). The diffusion rate of Fe element to titanium alloy is greater than the diffusion rate of Ti element to stainless steel at high temperature. The content of the Fe element increases with increasing depth, and the Ti element and the Fe

element are well mixed at the weld interface. The XRD analysis of the titanium alloy / steel welded joint is shown in Fig. 12. Due to the complex composition of the weld element and lattice distortion, the diffraction peak deviates from the standard position. It can be seen that the weld interface forms α -Ti phase, TiFe and TiFe₂ IMCs. The diffraction intensity of Ti₅Cr₇Fe₁₇ IMCs is insufficient because of its low content and uneven distribution in the interface. Therefore, the possible phase of the weld EDS results was not found on the XRD pattern.

Table 9. EDS results of the fusion zone and fracture (at.%)

Position	Ti	Fe	Al	V	Cr	Ni	Possible phase
1	78.24	8.07	7.22	3.40	1.95	1.11	α -Ti
2	65.20	18.93	6.09	2.63	3.44	3.70	α -Ti + TiFe
3	36.55	40.84	3.94	1.83	11.07	5.76	TiFe
4	56.83	25.52	4.94	2.72	7.61	2.83	α -Ti + TiFe
5	35.55	41.66	3.61	2.99	10.12	6.07	TiFe
6	27.76	50.09	1.31	2.57	12.13	6.13	TiFe ₂
7	16.51	64.96	-	0.22	19.33	7.84	Ti ₅ Cr ₇ Fe ₁₇
8	20.23	45.88	4.02	4.03	18.13	7.71	TiFe ₂
9	66.79	20.38	3.65	2.98	5.03	1.17	α Ti + TiFe
10	51.55	13.13	12.84	7.82	7.58	7.08	α Ti + TiFe

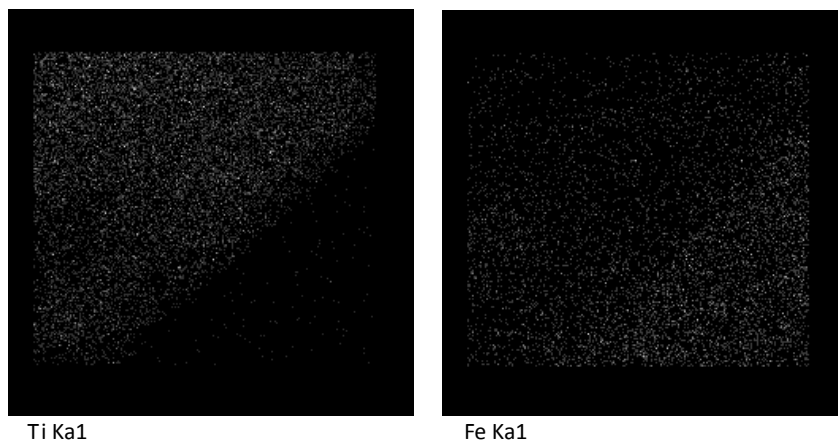


Fig. 11. EDS area scan

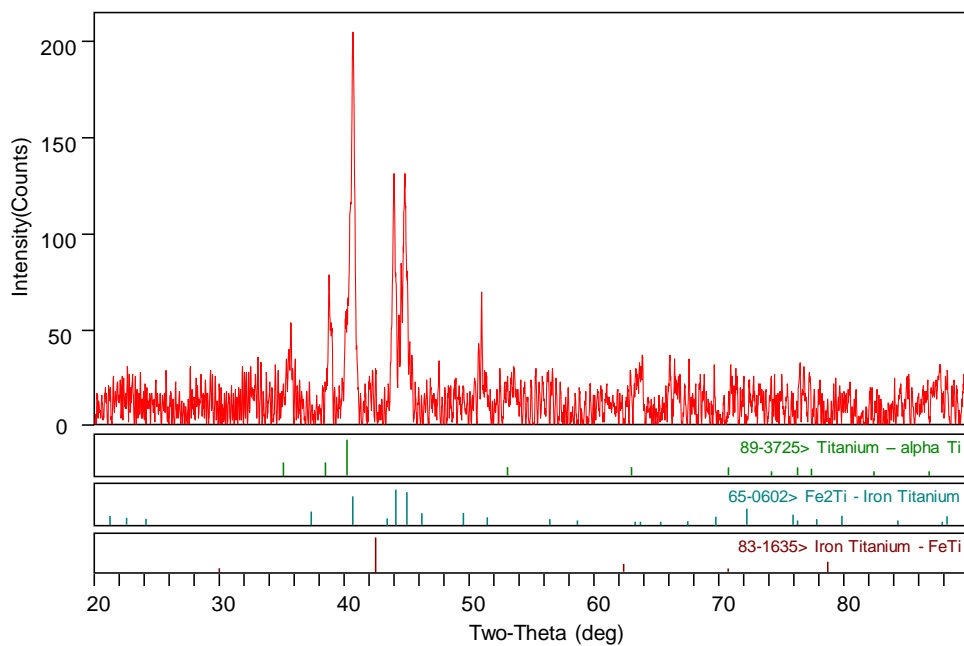


Fig. 12. XRD patterns of the joint

The Ti, Fe atoms of the welding interface area are thermally activated and free from the original lattice

during the welding process. The Fe atom with the smaller binding energy can break away first from the original

lattice structure into the titanium alloy matrix. When the Fe atom content in the Ti alloy matrix exceeds the solid solubility of Fe in Ti, the new nuclei are precipitated and lateral grown along the component interface to form the first phase $Ti_5Cr_7Fe_{17}$. When the first phase grows to a certain thickness along the direction perpendicular to the interface, the second phase nucleus is formed at its interface, that is, the nuclei of the $TiFe_2$ phase are formed on the phase interface of $Ti_5Cr_7Fe_{17}$. It can be deduced that the precipitation order of IMCs is $Ti_5Cr_7Fe_{17}$, C14_Laves ($TiFe_2$) and BCC_B2 ($TiFe$) during the welding of titanium alloy / steel dissimilar metals.

4.2. Tensile load and fractography

Fig. 13 shows the axial tensile force - displacement curve of the joint. The curve has no yield and necking

phenomenon. It is a typical brittle fracture curve with a peak breaking value 705.008N and a corresponding joint strength 58.75N / mm. The results of the fracture EDS are shown in Table 9. It is found that the fracture can be phase mixed with $\alpha Ti + TiFe + TiFe_2$, in which $TiFe$ and $TiFe_2$ are Ti-Fe IMCs. It can be deduced that the joint reaction layer has crack formation under the effect of welding residual stress. $TiFe$ IMC have a type B2 ordered body-centered cubic structure, which can be represented by two simple cubic cells that cross each other. $TiFe_2$ IMC have complex hexagonal MgZn₂ Laves structure, each unit has 8 Fe atoms and 4 Ti atoms. However, brittle cleavage faults often occur in BCC and HCP metals and alloys. It can be concluded that the joint will appear brittle cleavage fracture under normal stress, as shown in Fig. 13 b.

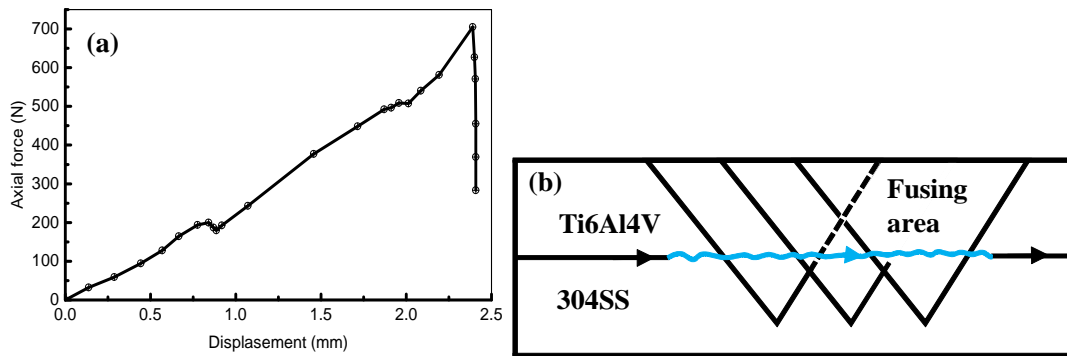


Fig. 13. Joint tensile curve and fracture path diagram. (a) tensile curve (b) fracture path diagram

Fig. 13 shows the fracture SEM of the welded joint on the titanium alloy side. The fracture is composed of a large number of river patterns, small area smooth surface and tear ridges, and the joint is a typical brittle cleavage fracture mode. The fracture occurs inside the fusing

region and forms a number of secondary cracks. Because of the rapid cooling after laser welding, the weld Ti-Fe IMCs cannot satisfy the stress generated by the deformation in the tensile test, and the stress is released only by the fracture.

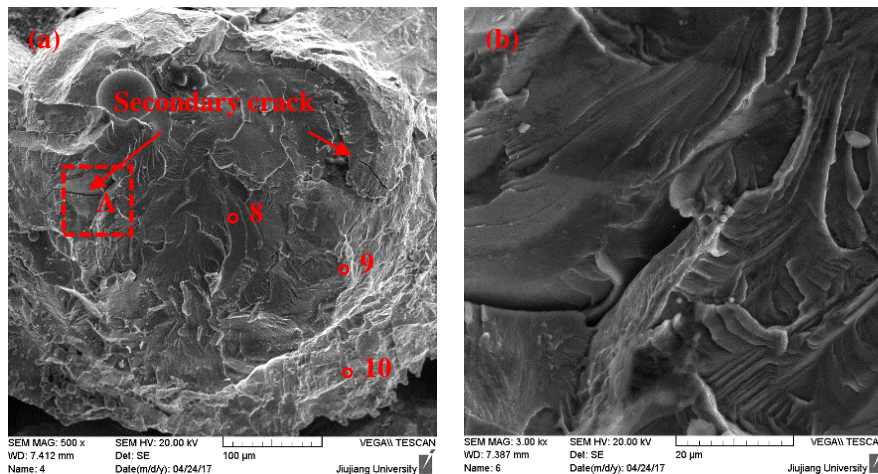


Fig. 14. Fracture morphologies. (a) Ti6Al4V side (b) magnification in the A area

5. Conclusions

From the foregoing analysis and discussion the following conclusion were summarized as following:

(1) Titanium alloy / steel dissimilar metal laser welding process parameters on the impact of the response has a very complex interaction. Different from the similar metal welding, to obtain the maximum limit strength requires longer pulse width, smaller pulse repetition rate and welding current.

(2) The weld surface of the titanium alloy / steel is slicked, the joint without macroscopic cracks, the maximum tensile load 705.008 N in the optimal conditions of welding current 122 A, pulse width 15 ms, pulse repetition rate 2 HZ, welding speed 50 mm / min, defocus amount -1 mm and positive and negative argon flow 15 L / min.

(3) The total thickness of the IMCs was about 40 μ m in lap interface. The intermediate reaction layer structure is divided into 3 layers, the gray band region adjacent to the titanium alloy side, the white band region in the middle layer, the acicular structure in the fusion zone and the stainless steel interface. The main formation phases are α -Ti, TiFe, TiFe₂ and a small amount of Ti₅Cr₇Fe₁₇ IMCs, and the precipitation order is Ti₅Cr₇Fe₁₇, C14_Laves (TiFe₂) and BCC_B2 (TiFe).

(4) There are more inconsistent height of the cleavage steps in the tensile fracture, showing brittle fracture characteristics. The fracture occurs inside the fusing region, breaking along the TiFe and TiFe₂ IMC layers, and the fracture forms many secondary cracks.

Acknowledgements

The authors gratefully acknowledge the financial support from the National High Technology Research and Development Program of China (grant nos. 2013AA041003), and the National Natural Science Foundation of China (grant nos. 51365039).

References

- [1] G. Welsch, R. Boyer, E. W. Collings, *Materials properties handbook: titanium alloys*, ASM international, The United States of America, 1994.
- [2] B. Shanmugarajan, G. Padmanabham, *Opt. Laser Eng.* **50**(11), 1621 (2012).
- [3] H. Lei, Y. B. Li, B. E. Carlson, Z. Lin, *J. Manuf. Sci. E-T. Asme.* **137**(5), (2015).
- [4] R. K. Shiue, S. K. Wu, C. H. Chan, C. S. Huang, *Metall. Mater. Trans. A* **37**(7), 2207 (2006).
- [5] R. K. Shiue, S. K. Wu, C. H. Chan, C. S. Huang, *Mat. Sci. Eng. A-Struct.* **488**(1-2), 186 (2008).
- [6] A. Elrefaey, L. Wojarski, W. Tillmann, *J. Mater. Eng. Perform.* **21**(5), 707 (2012).
- [7] A. Elrefaey, W. Tillmann, *J. Mater. Process. Technol.* **209**(5), 2746 (2009).
- [8] S. Kundu, S. Chatterjee, *Mater. Charact.* **59**(5), 631 (2008).
- [9] S. Kundu, S. Chatterjee, *Mat. Sci. Eng. A-Struct.* **527**(10-11), 2714 (2010).
- [10] M. Ghosh, S. Kundu, S. Chatterjee, B. Mishra, *Metall. Mater. Trans A* **36A**(7), 1891 (2005).
- [11] S. Kundu, M. Ghosh, A. Laik, K. Bhanumurthy, G. B. Kale, S. Chatterjee, *Mat. Sci. Eng. A-Struct.* **407**(1-2), 154 (2005).
- [12] S. Bozzi, A. L. Helbert-Etter, T. Baudin, B. Criqui, J. G. Kerbiguet, *Mat. Sci. Eng. A-Struct.* **527**(16-17), 4505 (2010).
- [13] W. U. Ming-Fang, S. I. Nai-Chao, J. Chen, *Trans. Nonferrous Met. Soc. China* **21**(5), 1035 (2011).
- [14] G. Liedl, R. Bielak, J. Ivanova, N. Enzinger, G. Figner, J. Bruckner, H. Pasic, M. Pudar, S. Hampel, *Phys. Procedia* **12**(1), 150 (2011).
- [15] M. J. Torkamany, S. Tahamtan, J. Sabbaghzadeh, *Phys. Procedia.* **31**(1), 458 (2010).
- [16] H. C. Chen, A. J. Pinkerton, L. Li, Z. Liu, A. T. Mistry, *Mater. Des.* **32**(2), 495 (2011).
- [17] J. Fan, C. Thomy, F. Vollertsen, *Phys. Procedia.* **12**, 134 (2011).
- [18] K. Fukatsu, *Weld Int.* **16**(8), 623 (2002).
- [19] S. Chen, M. Zhang, J. Huang, C. Cui, H. Zhang, X. Zhao, *Mater. Des.* **53**, 504 (2014).
- [20] Y. Zhang, D. Q. Sun, X. Y. Gu, H. M. Li, *Mater. Lett.* **185**, 152 (2016).
- [21] Y. Zhang, D. Q. Sun, X. Y. Gu, H. M. Li, *Int. J. Adv. Manuf. Tech.* **94**(1-4), 1073 (2018).
- [22] I. Tomashchuk, D. Grevey, P. Sallamand, *Mat. Sci. Eng. A-Struct.* **622**, 37 (2015).
- [23] I. Tomashchuk, P. Sallamand, H. Andrzejewski, D. Grevey, *Intermetallics* **19**(10), 1466 (2011).
- [24] I. Tomashchuk, P. Sallamand, N. Belyavina, M. Pilloz **585**, 114 (2013).
- [25] C. J. Wu, M. S. Hamada, *Experiments: planning, analysis, and optimization*, John Wiley & Sons, Canada, 2011.
- [26] D. Kim, S. Rhee, H. Park, *Int. J. Prod. Res.* **40**(7), 1699 (2002).
- [27] M. J. Torkamany, M. J. Hamed, F. Malek, J. Sabbaghzadeh, *J. Phys. D. Appl. Phys.* **39**(21), 4563 (2006).
- [28] S. Wang, K. Wang, G. Chen, Z. Li, Z. Qin, X. Lu, C. Li, *Calphad* **56**, 160 (2017).

*Corresponding author: zhangyf_lab@163.com